ACS OMEGA

http://pubs.acs.org/journal/acsodf

Article

Synthesis and Crystal Structures of Bis(diallydithiocarbamato)zinc(II) and Silver(I) Complexes: Precursors for Zinc Sulfide and Silver Sulfide Nanophotocatalysts

Peter A. Ajibade,* Thandi B. Mbuyazi, and Athandwe M. Paca

Cite This: *ACS Omega* 2023, 8, 24750−24760

Read Online

ACCESS | Metrics & More | Article Recommendations | Supporting Information

ABSTRACT: We report the preparation and crystal structures of bis(diallydithiocarbamato)zinc(II) and silver(I) complexes. The compounds were used as single-source precursors to prepare zinc sulfide and silver sulfide nanophotocatalysts. The molecular structure of bis(diallydithiocarbamato)zinc(II) consists of a dimeric complex in which each zinc(II) ion asymmetrically coordinates with two diallydithiocarbamato anions in a bidentate chelating mode, and the centrosymmetrically related molecule is bridged through the S-atom that is chelated to the adjacent zinc(II) ion to form a distorted trigonal bipyramidal geometry around the zinc(II) ions. The molecular structure of bis(diallydithiocarbamato)silver(I) formed a cluster complex consisting of a trimetric Ag_3S_3 molecule in which the diallydithiocarbamato ligand is coordinated to all the Ag(I) ions. The complexes were thermolyzed in dodecylamine, hexadecylamine, and octadecylamine (ODA) to prepare zinc sulfide and silver sulfide nanoparticles. The powder X-ray diffraction patterns of the zinc sulfide nanoparticles correspond to the hexagonal wurtzite while silver sulfide is in the acanthite crystalline phase. The high-resolution transmission electron microscopy images show that quantum dot zinc sulfide nanoparticles are obtained with particle sizes ranging between 1.98 and 5.49 nm, whereas slightly bigger silver sulfide nanoparticles are obtained with particle sizes of 2.70−13.69 nm. The surface morphologies of the ZnS and AgS nanoparticles capped with the same capping agent are very similar. Optical studies revealed that the absorption band edges of the as-prepared zinc sulfide and silver sulfide nanoparticles were blue-shifted with respect to their bulk materials with some surface defects. The zinc sulfide and silver sulfide nanoparticles were used as nanophotocatalysts for the degradation of bromothymol blue (BTB) and bromophenol blue (BPB). ODA-capped zinc sulfide is the most efficient photocatalyst and degraded 87% of BTB and 91% of BPB.

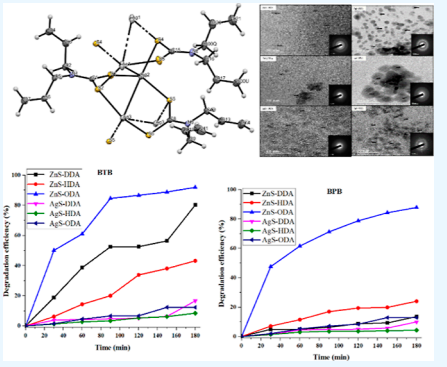

INTRODUCTION

Coordination compounds containing dithiocarbamate are a class of transition metal complexes that can be prepared using various synthetic methods.[1] In recent years, their potentials in a wide range of applications such as analytical chemistry, materials science, catalysis, and medicine[2,3] are being investigated. Interest in dithiocarbamate compounds is due to their ability to coordinate with different metal ions in different oxidation states and form different structural motifs.[4] The coordination behavior of each dithiocarbamate complex is paramount for their potential applications.[5] Metal dithiocarbamate complexes have been shown to be air stable and soluble in solvents such as dichloromethane, chloroform, water, and ethanol.[6] They possess unique properties such as electrophilicity, Lewis acidity, redox activity, valency, and radiochemical ability.[7] Metal complexes with sulfur-donor ligands have electrical conductivity, molecular magnetism, and electrochemical properties.[8] Thus, complexes of dithiocarbamate ligands have been applied in various applications such as in medicine and catalysis and as precursors for the preparation of metal sulfide nanoparticles.[9−11]

The use of illuminated semiconductors to decompose unwanted organic matter in water has received considerable interest in recent years.[12−14] Organic chemicals found as pollutants in industrial or household wastewater need to be removed before they are released into the environment. Such pollutants are also found in groundwater and surface water and must be treated to achieve acceptable drinking water quality. Therefore, it is important to identify the optimal treatment method for removing contaminants from wastewater. Photocatalytic decontamination of wastewater is a process that combines heterogeneous catalysis and UV/visible light technology.[15] The heterogeneous photocatalytic action of the semiconductor nanomaterial can lead to complete decontamination. Semiconductor photocatalysts such as metal sulfide have

Received: November 22, 2022
Accepted: March 27, 2023
Published: July 6, 2023

https://doi.org/10.1021/acsomega.2c07490
ACS Omega 2023, 8, 24750−24760

Table 1. Crystal Data and Structure Refinement Details for $[Zn_2(dalldtc)_4]$ (1) and $[Ag_3(dalldtc)_3]$ (2)

compounds	$[Zn_2(dalldtc)4]$	$[Ag_3(dalldtc)3]$
empirical formula	$C_{14}H_{20}N_2S_4Zn$	$C_{21}H_{30}Ag_3N_3S_6$
formula weight	409.93	840.45
temperature/K	99.98	102.84
crystal system	triclinic	monoclinic
space group	$\bar{P}1$	$P2_1/c$
a/Å	7.9470(3)	10.2956(3)
b/Å	9.4006(3)	15.0077(4)
c/Å	12.9509(5)	18.7727(5)
α/°	76.8860(10)	90
β/°	77.7450(10)	102.2400(10)
γ/°	77.7640(10)	90
volume/Å^3	907.08(6)	2834.69(14)
Z	2	4
ρ_{calc}g/cm^3	1.501	1.969
μ/mm^{-1}	6.127	20.721
F(000)	424.0	1656.0
crystal size/mm^3	0.405 × 0.28 × 0.155	0.22 × 0.165 × 0.1
radiation	CuKα (λ = 1.54178)	CuKα (λ = 1.54178)
2θ range for data collection/°	7.114 to 136.11	7.61 to 136.528
index ranges	$-9 \le h \le 9$, $-11 \le k \le 11$, $-15 \le l \le 15$	$-12 \le h \le 12$, $-18 \le k \le 18$, $-22 \le l \le 22$
reflections collected	19,533	42,980
independent reflections	3228 [Ri_{nt} = 0.0234, R_{sigma} = 0.0150]	5180 [Ri_{nt} = 0.0351, R_{sigma} = 0.0201]
data/restraints/parameters	3228/0/222	5180/0/346
goodness of fit on F^2	1.154	1.139
final R indexes [I> = 2σ (I)]	R_1 = 0.0214, wR_2 = 0.0540	R_1 = 0.0197, wR_2 = 0.0500
final R indexes [all data]	R_1 = 0.0219, wR_2 = 0.0545	R_1 = 0.0199, wR_2 = 0.0502
largest diff peak/hole/e Å−^{3}	0.24/−0.36	0.51/−0.84

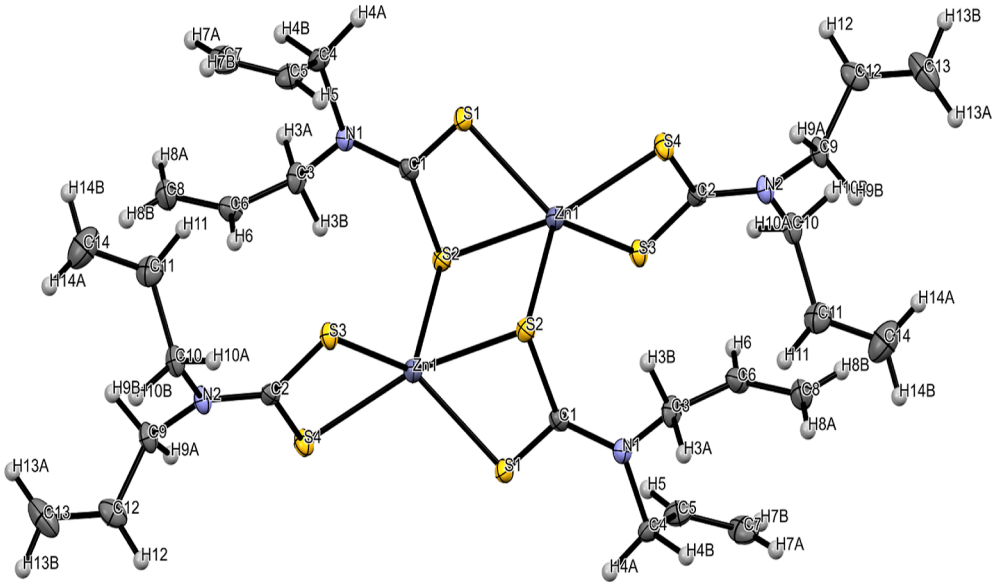

Figure 1. Molecular structure of $[Zn_2(dalldtc)_4]$ showing an atomic labeling displacement ellipsoid at 50% probability.

been applied in wastewater treatment.[16,17] Among some semiconductor photocatalysts, ZnS and Ag_2S nanoparticles with low bandgaps are efficient photocatalysts under irradiation with visible light source.[18,19]

Al-Shehri and co-workers evaluated the photocatalytic performance of Ag_2S nanoparticles, with energy bandgaps in the range of 1.014−1.026 eV, in methyl green dye under illumination of UV/visible light. The silver sulfide nanoparticles showed excellent photocatalytic behavior; hence, they can be used in water treatment applications.[20] The zinc sulfide nanoparticle has also been studied for its photocatalytic potential due to its relatively high potentials of conduction band electrons and valence band.[21] Recently, Aziz et al. prepared chitosan-capped zinc sulfide nanoparticles (CS-ZnS-NPs) and evaluated their use as a photocatalyst for the degradation of toxic dyes. At the optimum conditions, the nanoparticles degraded 96.7% of acid black 234 in 100 min and 92.6% of acid brown 98 in 165 min. The nanoparticles were easily recovered and recycled for four successive batches. In this study, we present the synthesis, characterization, and single-crystal X-ray structures of

https://doi.org/10.1021/acsomega.2c07490
ACS Omega 2023, 8, 24750−24760

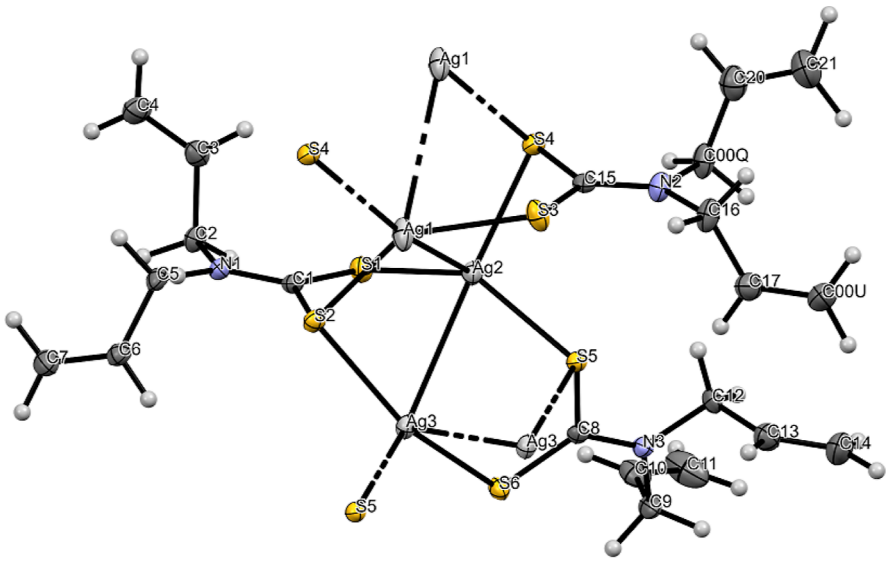

Figure 2. Molecular structure of $[Ag_3(dalldtc)_3]$ showing an atomic labeling displacement ellipsoid at 50% probability.

bis(diallydithiocarbamato)zinc(II) and bis-(diallydithiocarbamato)silver(I) complexes. The complexes were thermolyzed at 200 °C in dodecylamine (DDA), hexadecylamine (HDA), and octadecylamine (ODA) to prepare zinc sulfide and silver sulfide nanophotocatalysts. The potential of the as-prepared nanoparticles as photocatalysts was evaluated against bromothymol blue (BTB) and bromophenol blue (BPB) dyes.

RESULTS AND DISCUSSION

X-ray Crystal Structures of Zinc(II) and Silver(I) Dithiocarbamate Complexes. The crystal data and structure refinements for both bis(diallydithiocarbamato)zinc(II), $[Zn_2(dalldtc)_4]$, and bis(diallydithiocarbamato)silver(I), $[Ag_3(\mu\text{-dalldtc})_3]$, complexes are presented in Table 1, while selected bond lengths and bond angles for the compounds are presented in Table T1. $[Zn_2(dalldtc)_4]$ (Figure 1) crystallized in a triclinic space group $P\bar{1}$ with $Z = 2$ in which $[Zn_2(dalldtc)_4]$ is at the center of an inversion to form a dimeric zinc(II) complex. Each Zn(II) ion in the asymmetric unit is coordinated to two molecules of diallydithiocarbamato anions that act as bidentate chelating ligands and bridged through the S-atom of the adjacent diallydithiocarbamato anion. The geometry around each Zn(II) ion can be described as a distorted trigonal bipyramidal geometry which consists of two bidentate diallydithiocarbamato anions and the sulfur atom of one of the ligands that coordinated to the other Zn(II) ion in the dimeric complex. The distortion imposed on the geometry is due to the S(1)−Zn(1)−S(2) and S(3)−Zn(1)−S(4) chelate angles of 69.31(12)° and 75.56(13)°, respectively. The S−Zn(1)—S dithiocarbamato bite angles deviate significantly from 90°. The deviations of the S−Zn(1)—S bite angles cause the deviation of other angles such as $S2^1$−Zn1−S4 [109.723(15)], S(3)−Zn(1)−$S(2^1)$ [115.686(15)], and S(1)−Zn(1)−$S(2^1)$ [105.092(15)] that deviate from the ideal value of 91.164(3)°, which is significantly different from the ideal value. The angles described by the atoms in the equatorial positions should be close to 120°; the angles involving S(3)#1 atoms [115.902(15) and 135.540(16)] are smaller than the ideal value (120°), but the S1−Zn1−S4 106.879(15) bond angle is somewhat smaller most probably due to the steric requirements of the ligands, and the S(2)−Zn(1)−S(4) bond angle of 156.686(14)° deviates from the ideal value of 180°. The structure of the zinc(II) complex is similar to the structure of the other dithiocarbamate zinc(II) complex with different functional groups.[22−25]

$[Ag_3(dalldtc)_3]$ (Figure 2) crystallized in a monoclinic space group $P2_1/c$. The molecular structure of the silver(I) complex consists of $[Ag_3(dalldtc)_3]$ in the asymmetric molecules in which three Ag(I) ions and three molecules of diallydithiocarbamato ligands are coordinated to form a metal cluster consisting of a trimetric Ag_3S_3 molecule in which the diallydithiocarbamato ligand is coordinated to all the Ag(I) ions. Each diallydithiocarbamato ligand in the silver(I) cluster is bonded to three Ag(I) ions through the sulfur atoms with one sulfur atom covalently bonded while the other sulfur atoms act as two electrons-three centers within the metal cluster. Each Ag(I) ion is linked to three Ag(I) ions through a Ag2−Ag1 bond distance of 2.9808(2) and a Ag1−$Ag1^2$ bond distance of 3.1160(4) Å.[26]

In both cases, the AgS_3 bite angle is essentially trigonal planar with S−Ag−S bond angles of 143.59(2), 112.05(2), and 103.215(18) for Ag(I); 140.571(19), 116.824(19), and 99.675(18) for Ag(2); and 150.887(19), 115.679(18), and 92.713(1) for Ag(3). These bond angles deviate from the ideal trigonal planar arrangement. The Ag...Ag interactions point out of this plane and are not orthogonal. The other two Ag...Ag distances are long but are only interactions (3.3210(5) and 3.3465(5) Å) which are shorter than the sum of two silver atoms. *Van der Waals* (3.44 Å) signifies the presence of the Ag−Ag metallophilic bond.[27]

Spectroscopic Studies. The FTIR spectra of $[Zn_2(dalldtc)_4]$ and $[Ag_3(dallydtc)_3]$ (Figure S3) showed the characteristic peaks of the dithiocarbamate moiety. The ν(N−C) bands observed at 1472 and 1458 cm^{-1} for $[Zn_2(dalldtc)_4]$ and $[Ag_3(dalldtc)_3]$, respectively, signify the partial carbon−nitrogen double-bond characteristic of the dithiocarbamate anion. The bands at 985 cm^{-1} for $[Zn_2(dalldtc)_4]$ and at 979 cm^{-1} for $[Ag_3(dalldtc)_3]$ are due to the $\nu(-CS_2)$ stretching vibrations which indicate that dithiocarbamates acts as bidentate chelating ligands. The absorption spectra of the two complexes are shown in Figure S4. $[Zn_2(dalldtc)_4]$ exhibits two bands, at 264 and 284 nm, which are ascribed to the $\pi \rightarrow \pi^*$ intra-ligand and metal−ligand charge-transfer (MLCT) transitions.

https://doi.org/10.1021/acsomega.2c07490
ACS Omega 2023, 8, 24750−24760

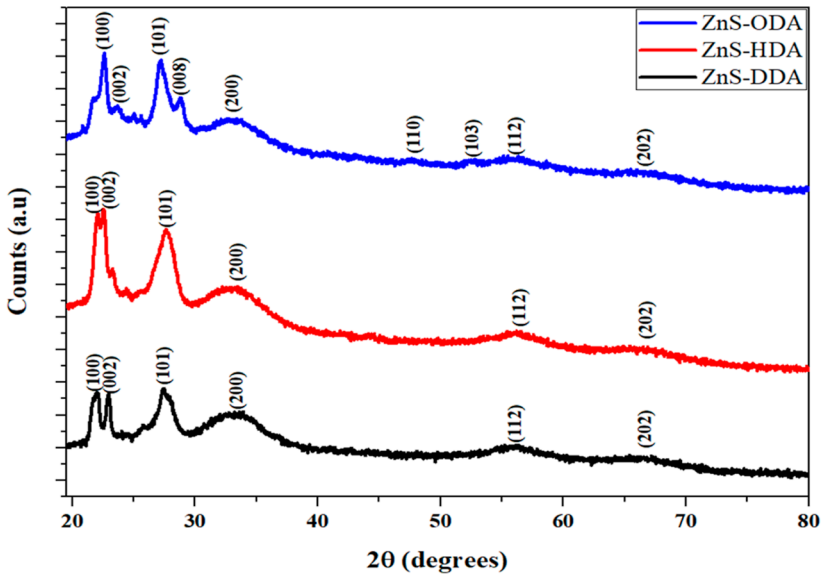

Figure 3. Powder X-ray diffraction patterns of the ZnS nanoparticles.

$[Ag_3(dalldtc)_3]$ shows one broad band at 279 nm, which is attributed to the $\pi \rightarrow \pi^*$ intra-ligand charge-transfer transition due to the thioureide moiety of the dithiocarbamate ligand.[19]

Powder X-ray Diffraction of Zinc Sulfide and Silver Sulfide Nanoparticles. The powder X-ray diffraction patterns of the ZnS nanoparticles are presented in Figure 3. The ZnS−DDA and ZnS−HDA patterns showed six peaks at 22.08, 22.96, 27.65, 33.24, 56.18, and 66.87° which are indexed to (100), (002), (101), (200), (112), and (202) planes, respectively. The ZnS−ODA diffraction patterns show nine peaks at 22.61, 23.30, 27.21, 28.85, 33.26, 47.82, 52.55, 56.29°, and 66.25° which correspond to (100), (002), (101), (008), (200), (110), (103), (112), and (202) planes, respectively. All the diffraction peaks of ZnS nanoparticles correspond with the standard values of hexagonal wurtzite zinc sulfide (JCPDS card no. 39−1363).[28,29] The differences in the diffraction patterns and the number of peaks could be ascribed to the different capping agents used to prepare the nanoparticles. The broad diffraction peaks observed could be attributed to the small particle sizes of the as-prepared zinc sulfide nanoparticles.[30]

The powder X-ray diffraction patterns of the silver sulfide nanoparticles are presented in Figure 4. The as-prepared silver sulfide nanoparticles showed a monoclinic/acanthite (α-Ag_2S) crystalline phase (JCPDS card no. 14−0072).[31,32] Ag_2S−DDA shows diffraction peaks at 20.78, 21.49, 23.45, 30.64, 36.87, 40.65, 50.68, and 53.67° corresponding to the (−101), (110), (−111), (−112), (112), (031), (014), and (−213) facets, respectively. The Ag_2S−HDA diffraction pattern shows reflections from the (−101), (110), (111), (−112), (112), (031), (200), (014), and (200) planes. The Ag_2S−ODA diffraction patterns also show peaks at 20.54, 22.41, 23.79, 27.73, 36.54, 40.49, 50.62, and 53.56° corresponding to the (−101), (110), (−111), (−112), (112), (031), (014), and (−213) planes. The high-intensity peaks indicate that the as-prepared Ag_2S nanoparticles are crystalline.[33]

Morphological Studies of the ZnS and AgS Nanoparticles. High-resolution transmission electron microscopy (HRTEM) and scanning electron microscopy (SEM) were used to study the morphological properties of the as-prepared nanoparticles. The HRTEM images and SAED patterns of the as-prepared nanoparticles are shown in Figure 5. Quantum dots

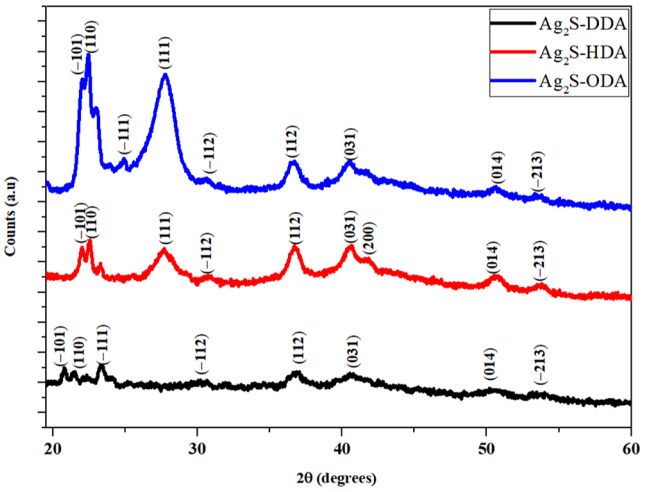

Figure 4. Powder X-ray diffraction patterns of the Ag_2S nanoparticles.

are observed in the HRTEM micrograph of the as-prepared ZnS nanoparticles. The ZnS-DDA nanoparticles have particle sizes in the range of 2.17−5.49 nm, while ZnS-HDA and ZnS-ODA nanoparticles have particle sizes of 1.98−2.81 and 2.03−3.51 nm, respectively. The SAED patterns of ZnS-DDA and ZnS-ODA show diffused rings which indicate that the nanoparticles have a polycrystalline nature, which could be ascribed to overload of thickness for the electron diffraction.[34] The SAED patterns of ZnS-HDA show a single-crystal nature.[35]

The HRTEM images and SAED patterns of the as-prepared nanoparticles are shown in Figure 6. The HRTEM micrographs of the Ag_2S-DDA nanoparticles showed spherically shaped particles with sizes of 8.64−12.58 nm, and the SAED patterns of Ag_2S-DDA showed partially diffused rings with bright spots, which indicate that the nanoparticles are both monocrystalline and polycrystalline. Ag_2S-HDA nanoparticles have particle sizes in the range of 7.07−13.69 nm, and the SAED patterns show diffused rings with no spots, which indicates that the as-prepared silver sulfide nanoparticles are also polycrystalline in nature. The micrographs show that Ag_2S-ODA nanoparticles have a particle size of 2.70−7.32 nm. The SAED patterns of Ag_2S-ODA show

https://doi.org/10.1021/acsomega.2c07490
ACS Omega 2023, 8, 24750−24760

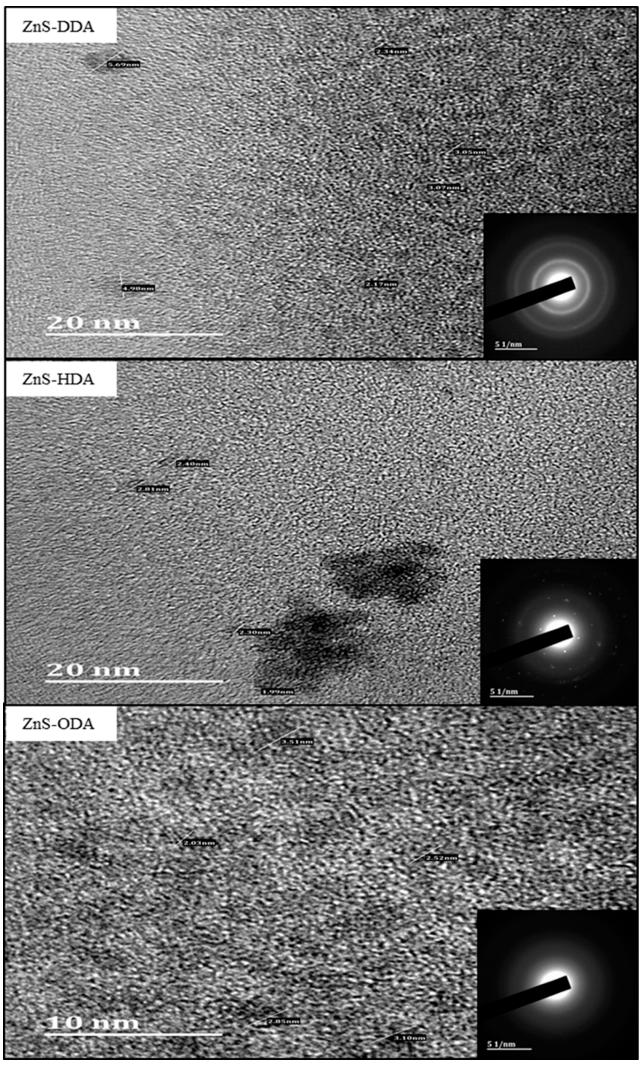

Figure 5. HRTEM images and inserted SAED patterns of ZnS-DDA, ZnS-HDA, and ZnS-ODA nanoparticles.

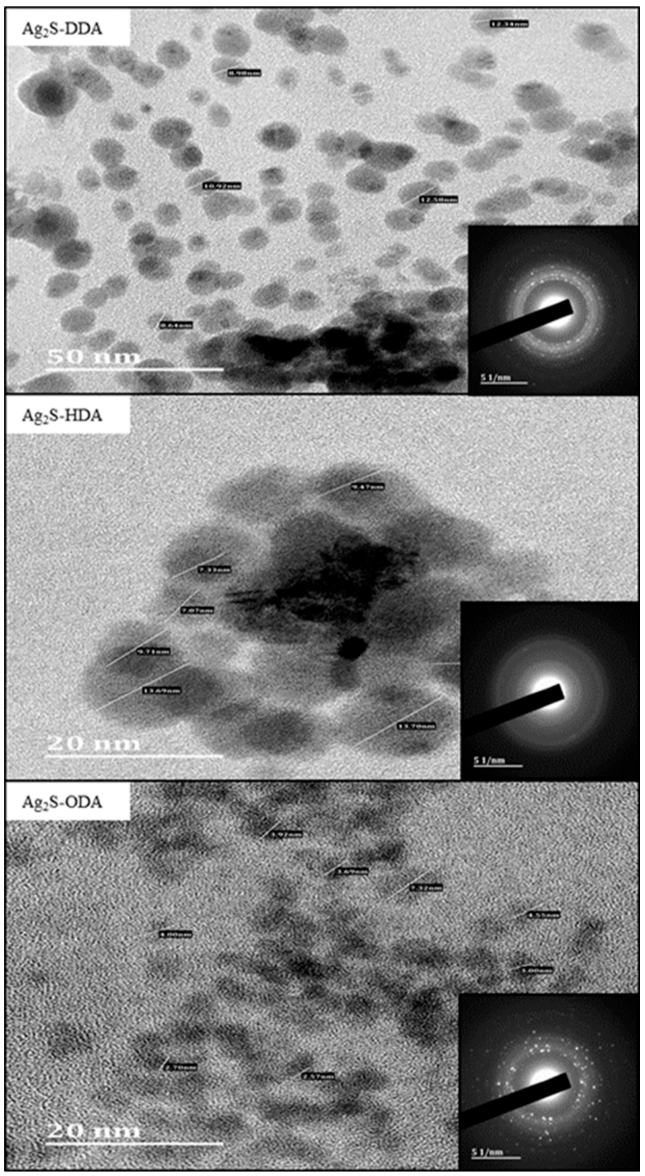

Figure 6. HRTEM images and inserted SAED patterns of Ag_2S-DDA, Ag_2S-HDA, and Ag_2S-ODA nanoparticles.

bright spots with no ring, showing that the nanoparticles are crystalline in nature.

The surface morphologies of the as-prepared nanoparticles were studied using SEM (Figure S5). The nanoparticles capped with the same capping agent show very similar surface morphologies. ZnS and Ag_2S nanoparticles capped with DDA show a flake-like morphology. The HDA-capped ZnS and Ag_2S nanoparticles exhibit sponge-like morphologies that look like a ball. Rough flake-like surfaced morphologies were observed for nanoparticles capped with the ODA capping agent. The different surface morphologies observed for the different capping agents suggest that the surface of the nanoparticles is influenced by the capping agent irrespective of the single-source precursor.

Optical Properties of the Zinc Sulfide and Silver Sulfide Nanoparticles. UV−Vis and photoluminescence spectroscopies were used to study the optical properties of the as-prepared nanoparticles (Figure S6) and show the absorption band edges of the ZnS and Ag_2S nanoparticles. The absorption band edges are observed at 288, 285, and 286 nm for ZnS-DDA, ZnS-HDA, and ZnS-ODA nanoparticles, respectively. The absorption band edges of the Ag_2S nanoparticles appeared at 286, 286, and 285 nm for Ag_2S-DDA, Ag_2S-HDA, and Ag_2S-ODA nanoparticles, respectively. The optical bandgap of the nanoparticles was estimated using the Tauc plots (Figure S7). The estimated optical bandgaps (E_g) for the ZnS-DDA, ZnS-HDA, and ZnS-ODA nanoparticles are 4.04, 4.10, and 4.08 eV, respectively. The E_g are blue-shifted in comparison to their bulk materials (ZnS = 3.6 eV),[36] indicating the quantum confinement of the as-prepared nanoparticles. The E_g of Ag_2S nanoparticles are 3.97, 3.51, and 3.32 eV for Ag_2S-DDA, Ag_2S-HDA, and Ag_2S-ODA, respectively. The AgS nanoparticles are also blue-shifted and have a much higher bandgap compared to their bulk material (AgS = 0.9 eV),[19] which confirmed that they are small as can be seen from the HRTEM images.

The photoluminescence spectra of the ZnS and Ag_2S nanoparticles are presented in Figure S8. Three emission peaks are observed in all the as-prepared nanoparticles. The first peak observed at 297 and 295 nm for ZnS and Ag_2S nanoparticles, respectively, could be associated with band−band transitions, and the values are almost equal to the band edges of the nanoparticles.[37] The middle high intense and broad

https://doi.org/10.1021/acsomega.2c07490
ACS Omega 2023, 8, 24750−24760

emission peaks observed at 384 and 387 nm for ZnS and Ag_2S nanoparticles, respectively, could be ascribed to free-exciton recombination.[36] The third emission peak is assigned to the transition from the conduction band to the sulfur vacancy level and surface defects.[36,38]

Photocatalytic Degradation of BPB and BTB Dyes by ZnS and AgS Nanoparticles. The results of the photocatalytic degradation of the BTB and BPB dyes in the presence of ZnS and Ag_2S nanoparticles under visible light irradiation are presented in Figure 7. There was negligible degradation of

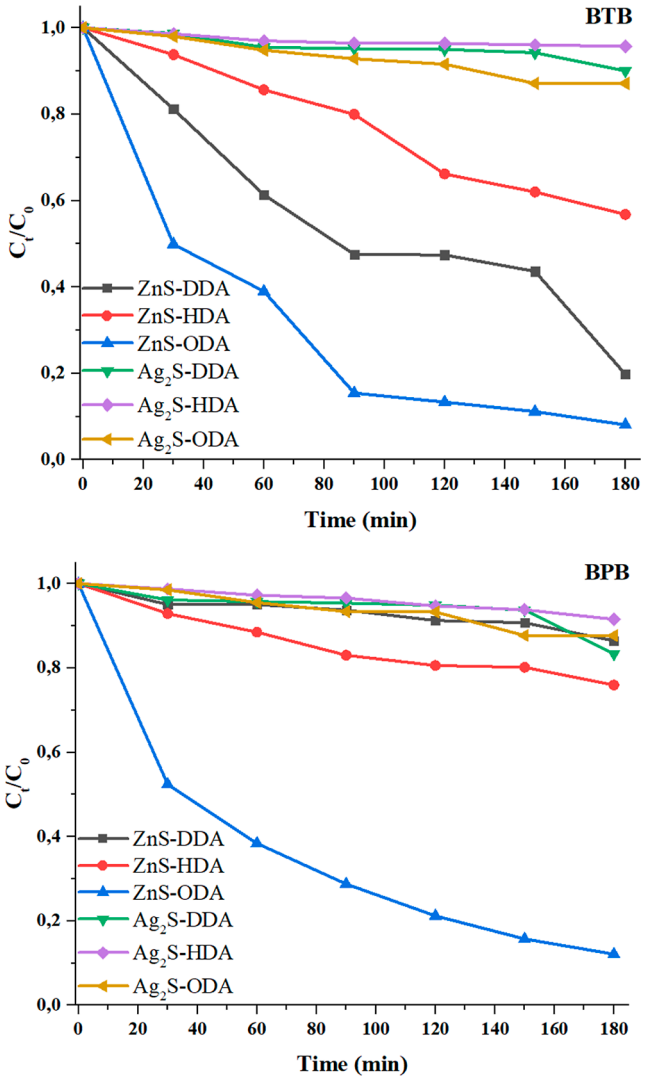

Figure 7. Effect of time on BTB and BPB degradation.

dyes in the absence of ZnS and Ag_2S nanoparticles. The results show that the concentrations of the dyes continuously decrease as the irradiation time increased. This indicates that the photocatalytic degradation of BTB and BPB dyes is time dependent and increases with increasing irradiation time.[39]

The photocatalytic degradation efficiency percentage plots (Figure 8) show that Ag_2S-DDA, Ag_2S-HDA, and Ag_2S-ODA degraded 87.86, 24.05, and 13.57% of BPB dye after 180 min. On the other hand, under similar conditions, only 12.37, 8.45, and 16.65% of BPB were degraded by Ag_2S-DDA, Ag_2S-HDA, and Ag_2S-ODA nanoparticles, respectively. This indicates that ZnS-ODA has the highest photocatalytic efficiency among the as-prepared nanoparticles against BPB dyes. The enhanced photocatalytic degradation efficiency of ZnS-ODA may be attributed to its smaller particle size, which translates to a large surface area, that permits more interactions with the dye molecule.[40]

The photocatalytic degradation efficiencies of bromothymol (BTB) by ZnS-DDA, ZnS-HDA, and ZnS-ODA have been found to be 80.20, 43.21, and 91.91%, respectively, after 180 min of irradiation. However, the photocatalytic degradation of BTB was found to be lower in the case of Ag_2S-DDA (12.89%), followed by Ag_2S-ODA (9.98%) and Ag_2S-HDA (4.30%), under the same experimental conditions. Thus, it showed that the ZnS-ODA and ZnS-DDA nanoparticles exhibited higher photocatalytic activity toward the degradation of BTB compared to ZnS-HDA and all the Ag_2S nanoparticles. ZnS-HDA results are comparable to other HDA-capped ZnS nanoparticles.[41] Ag_2S nanoparticles exhibited low photocatalytic activity toward BTB and BPB, which may be attributed to the high recombination rate of photogenerated charges.[42]

The kinetics of photocatalytic degradation of BPB and BTB by the ZnS and Ag_2S nanoparticles has been described using the Langmuir−Hinshelwood model.[43,44] Figure 8 shows the plot of $\ln(C_t/C_0)$ over irradiation time for BTB and BPB dye degradation in the presence of ZnS and Ag_2S nanoparticles. The photocatalytic degradation of BTB and BPB follows a pseudo-first-order kinetic model, and the rate constants (k/min) with their corresponding correlation coefficients (R^2) calculated from the plots are presented in Table 2. The highest degradation rate of 0.0111 min^{-1} for BPB and 0.01382 min^{-1} for BTB was accomplished by ZnS-ODA among the other photocatalysts, which are consistent with the degradation efficiency curves.

Photostability Studies of ZnS Nanoparticles. Based on the results obtained for the photocatalytic degradation of BPB and BTB by the as-prepared ZnS and Ag_2S nanophotocatalysts, ZnS nanoparticles were chosen for reuse due to their higher photocatalytic activity (Figure 9). As the photocatalytic reaction cycles were increased, a slight decline of about 0.62−1.09% in the nanophotocatalyst activity toward the degradation of BTB was observed. The little decrease in activity could be due to the loss of catalyst during the experiment. The percentage of BPB dye degradation also decreased as the number of photocatalytic reaction cycles increased with a difference of 2.45−4.93%. The decline in the percentage degradation of BPB after four cycles could be caused by the dye molecules occupying the active sites of the catalyst[30] and the photocorrosion of ZnS nanoparticles.[45] The overall results show that ZnS nanoparticles can be reused for at least four cycles of photocatalytic degradation reactions while maintaining high levels of activity.

CONCLUSIONS

Bis(diallydithiocarbamato)zinc(II) and silver(I) complexes were synthesized and characterized by spectroscopic techniques and single-crystal X-ray crystallography. The molecular structure of bis(diallydithiocarbamato)zinc(II) revealed a binuclear compound in which each zinc(II) ion bidentately coordinates with two molecules of diallydithiocarbamato anions, and the centrosymmetrically related molecules are bridged through the Zn···S bond to form a distorted trigonal bipyramidal geometry around the zinc(II) ions. Bis(diallydithiocarbamato)Ag(I) crystallized as $[Ag_3(dalldtc)_3]$ in which the three Ag(I) ions and three molecules of diallydithiocarbamato anions coordinate to form an asymmetric metal cluster with a trimetric Ag_3S_3 core in which the diallydithiocarbamato anions are coordinated to all

https://doi.org/10.1021/acsomega.2c07490
ACS Omega 2023, 8, 24750−24760

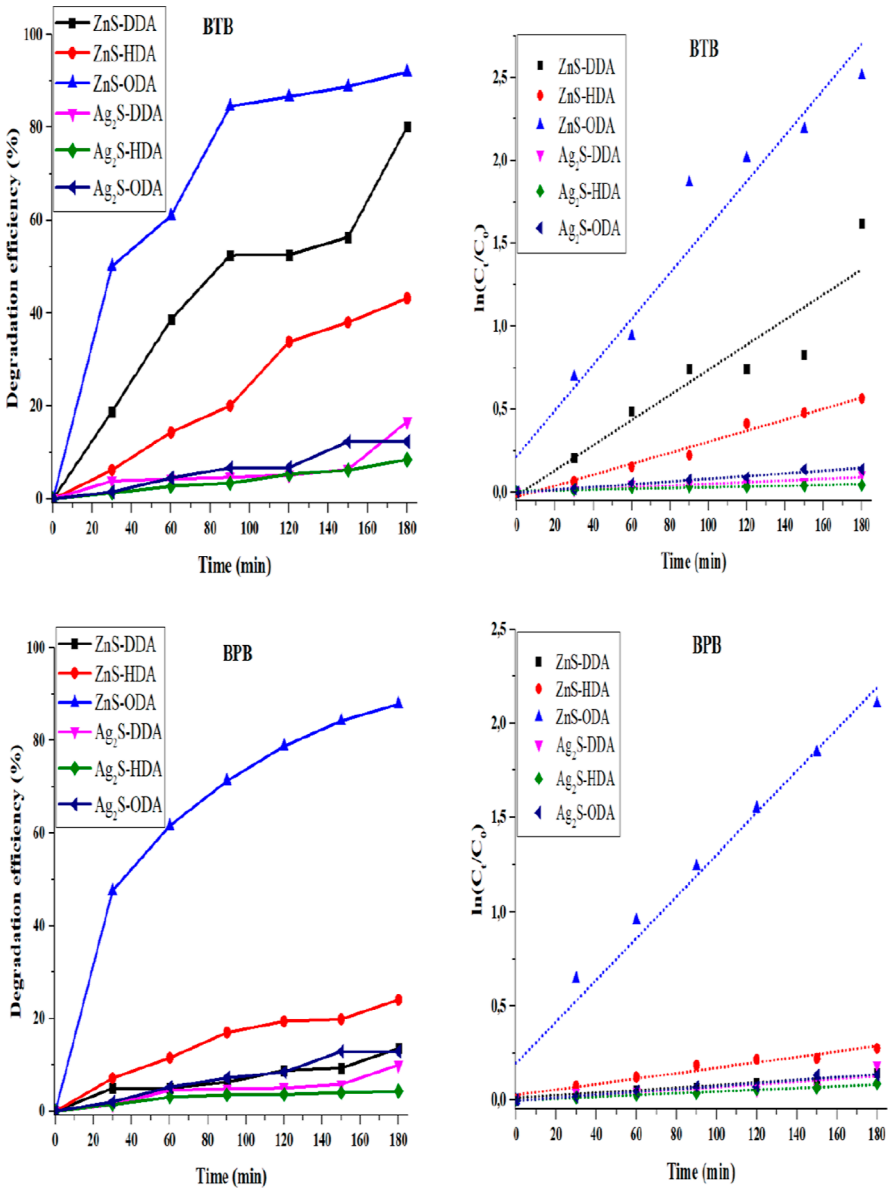

Figure 8. Degradation efficiency curves of BTB and BPB by ZnS and Ag_2S nanoparticles and their corresponding kinetic plots.

Table 2. Photocatalytic Degradation Percentage of BPB and BTB, Rate Constants of Photodegradation, and Its Corresponding Correlation Coefficient

dyes	catalyst	degradation efficiency (%)	rate constant (min−1)	R^2
BPB	ZnS-ODA	87.86	0.0111	0.9774
	ZnS-HDA	24.05	0.00145	0.9767
	ZnS-DDA	13.57	6.81×10^{-4}	0.9619
	Ag_2S-ODA	12.37	7.76×10^{-4}	0.9744
	Ag_2S-HDA	8.45	4.68×10^{-4}	0.9840
	Ag_2S-DDA	16.65	7.21×10^{-4}	0.8223
BTB	ZnS-ODA	91.91	0.01382	0.9428
	ZnS-HDA	43.21	0.00331	0.9814
	ZnS-DDA	80.20	0.00757	0.8843
	Ag_2S-ODA	12.89	8.14×10^{-4}	0.9733
	Ag_2S-HDA	4.30	2.27×10^{-4}	0.9214
	Ag_2S-DDA	9.98	4.91×10^{-4}	0.8817

the Ag(I) ions. Each diallydithiocarbamato anion in the silver(I) cluster is bonded to three Ag(I) ions through the sulfur atoms with one sulfur atom covalently bonded, while the other sulfur atoms act as two electrons-three centers within the metal cluster. Each Ag(I) ion is linked to three Ag(I) ions through a Ag2−Ag1 bond distance of 2.9808(2) and a Ag1−Ag1[2] bond distance of 3.1160(4) Å. The complexes were thermolyzed in DDA, HDA, and ODA to prepare zinc sulfide and silver sulfide nano-photocatalysts for the degradation of BTB and BPB. The powder XRD diffraction patterns of the zinc sulfide nanoparticles confirmed a hexagonal wurtzite crystalline phase while silver sulfide is in the monoclinic/acanthite crystalline phase. The HRTEM micrographs of the zinc sulfide revealed spherical particles with particle sizes in the quantum dot range of 1.98−5.49 nm, while slightly bigger particles were obtained for silver sulfide nanoparticles with particle sizes of 2.70−13.69 nm. The SEM images showed that the capping agents influence the surface morphologies of the as-prepared ZnS and AgS nanoparticles. The potential of the as-prepared nanoparticles as photocatalysts was evaluated against BTB and BPB dyes.

https://doi.org/10.1021/acsomega.2c07490
ACS Omega 2023, 8, 24750−24760

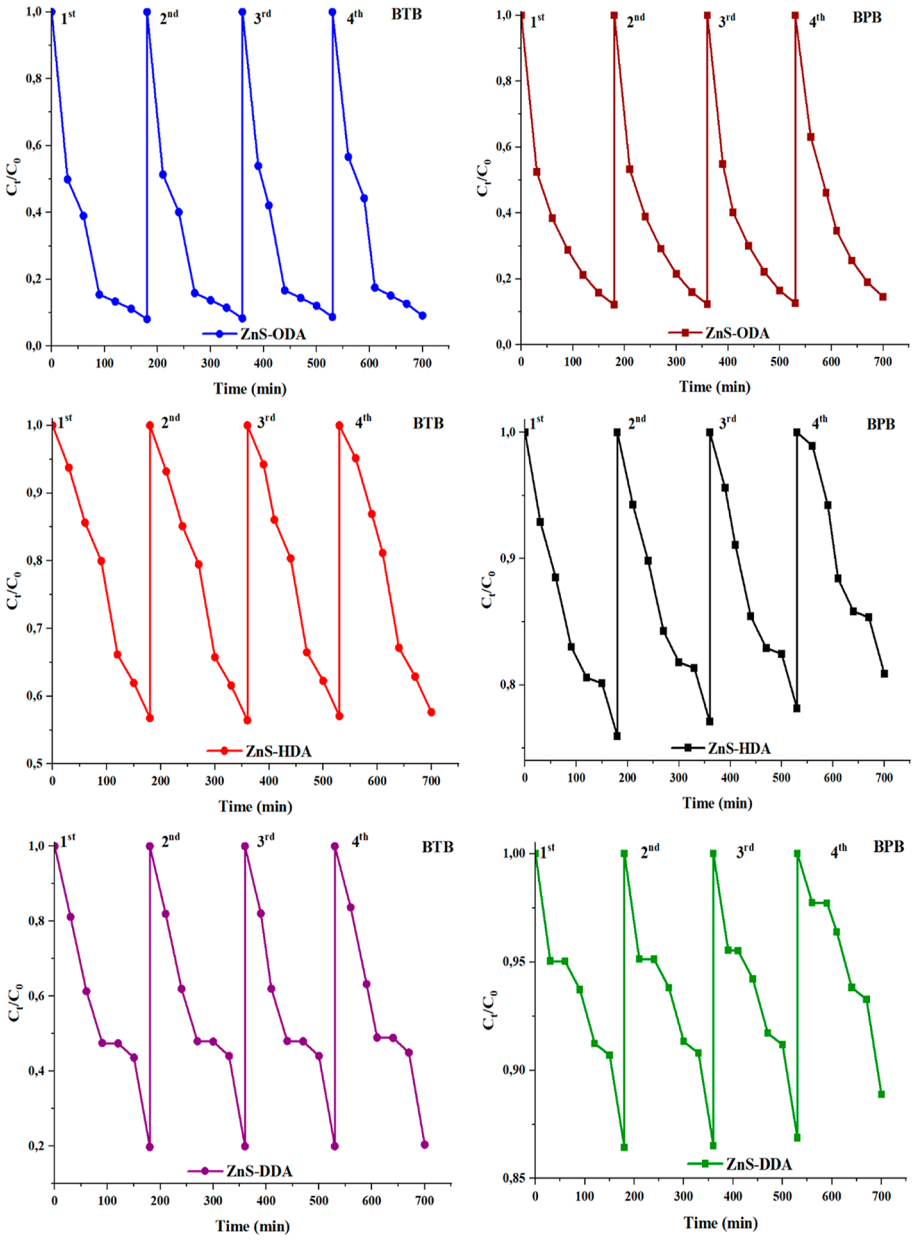

Figure 9. Recyclability test of the as-prepared ZnS catalysts on BTB and BPB.

Photocatalytic degradation studies show that ODA-capped zinc sulfide nanoparticles are the most efficient photocatalysts and degraded 87% of BTB and 91% of BPB.

EXPERIMENTAL SECTION

Materials. Analytical grades of all chemicals and solvents used were purchased from Merck Chemical and used without further purification. The ligand was prepared following a reported procedure.[49]

Synthesis of Zinc(II) and Silver(I) Dithiocarbamate Complexes. An aqueous solution of potassium diallyldithiocarbamate (2.1 g, 10 mmol) was added to $ZnCl_2$ (0.68 g, 5 mmol) or $AgNO_3$ (1.7 g, 10 mmol) dissolved in 20 mL of distilled water and vigorously stirred at room temperature for 4 h. The resultant precipitate was filtered, washed several times with water and finally with methanol, and vacuum-dried.

[Zn(dalldtc)$_2$]. Color: white, Yield (%): 61. Molecular mass (m/z): 409.95, Calcd for $C_{14}H_{20}N_2S_4Zn$ $[M]^+$: Found: 409.98. Selected FTIR, $\nu(cm^{-1})$: N−C (1472), C−S (1230), C═S (1099). ^{1}H NMR (400 MHz, (DMSO-d_6, δ (ppm)): 5.91−5.83 (m, 2H, −CH−), 5.26−5.21 (d, 4H, $-CH_2$), 4.43−4.41 (d, 4H, $-NCH_2-$). ^{13}C NMR (400 MHz, (DMSO-d_6, δ (ppm)): 205.86 (C−S), 131.78 (−CH−), 118.92 ($-CH_2$), 56.53 ($-NCH_2-$). Anal. Calcd for. $[Zn(S_2CNC_6H_{10})_2]$: C, 41.02; H, 4.92; N, 6.83; S, 31.28. Found: C, 41.15; H, 4.87; N, 6.78; S, 31.17.

[Ag(dalldtc)]. Color: Yellow, Yield (%): 73. Molecular mass (m/z): 280.15, Calcd for $C_7H_{10}NS_2Ag$ $[M]^+$: Found: 280.93. Selected FTIR, $\nu(cm^{-1})$: N−C (1458), C−S (1217), C═S (1089). ^{1}H NMR (400 MHz, (DMSO-d_6, δ (ppm)): 5.96−5.87 (m, 2H, −CH−), 5.28−5.21 (d, 4H, $-CH_2$), 4.59−4.57 (d, 4H, $-NCH_2-$). ^{13}C NMR (400 MHz, (DMSO-d_6, δ (ppm)): 205.61 (C−S), 131.68 (−CH−), 119.02 ($-CH_2$), 58.72 ($-NCH_2-$). Anal. Calcd for. $[Ag(S_2CNC_6H_{10})]$: C, 30.01; H, 3.60; N, 5.00; S, 22.89. Found: C, 29.98; H, 4.3.57; N, 4.89; S, 22.77.

https://doi.org/10.1021/acsomega.2c07490
ACS Omega 2023, 8, 24750−24760

Single-Crystal X-ray Structure Determination. Suitable crystals of the compounds were obtained from the solution of dichloromethane/acetonitrile. The single-crystal data of the complex were obtained on a Bruker SMART APEX2 area detector diffractometer using MoK_a. The crystal temperature was maintained at 100(2) K during data collection. Using Olex2[46] as a molecular graphical interface, the structure was solved with the ShelXS-2013[47] structure solution program using the direct solution method. The structure was refined with version 2016/6 of ShelXL[48] using least-squares minimization.

Preparation of Zinc Sulfide and Silver Sulfide Nanoparticles. A modified literature method was used.[49−51] The DDA, HDA, or ODA (2 g) capping agent was heated to 200 °C in a three-necked flask fitted with a reflux condenser, a thermometer, and a rubber septum. $[Zn_2(dalldtc)_4]$ or $[Ag(\mu\text{-}dalldtc)_3]$ (0.2 g) dispersed in oleic acid (2 mL) was injected to the hot capping agent. The reaction was maintained at 200 °C for 1 h under a N_2 flow. It was cooled to about 60 °C and cold methanol was added. The resultant precipitate was separated by centrifugation and washed several times with cold methanol. The nanoparticles were dried under vacuum. The as-prepared nanoparticles were labeled ZnS-DDA, ZnS-HDA, and ZnS-ODA for nanoparticles prepared from $[Zn_2(dalldtc)_4]$ and AgS-DDA, AgS-HDA, and AgS-ODA for nanoparticles prepared from $[Ag(\mu\text{-}dalldtc)_3]$.

Photocatalytic Activity of the Nanoparticles. The photocatalytic degradation efficiency of the ZnS and Ag_2S nanoparticles was assessed by monitoring the degradation of BTB and BPB under visible light. The experiment was carried out in a continuous swirling OSRAM VIALOX 70 W incandescent mercury lamp. 40 mg of each nanoparticle was dispersed into 40 mL of 20 mg/L BTB or BPB solution. To achieve adsorption−desorption equilibrium, the solution was sonicated for 30 min and magnetically agitated in the dark for 60 min. Then, the solution was exposed to light for 180 min. 5 mL aliquots of the sample were collected at 30 min intervals and filtered, and the filtrate was taken for absorption analysis. Equation 1 was used to calculate the degradation efficiency[43]

$$D = \frac{C_0 - C_t}{C_0} \times 100 \quad (1)$$

where D is degradation efficiency and C_0 and C_t are the initial and final concentrations of BTB and BPB solutions, respectively. The reusability and stability of the catalysts were evaluated by recycling them four times. After each run, the catalyst was filtered, washed with water and ethanol, and then dried in an oven at 80 °C for 2 h.

Characterization Techniques. FTIR spectra were recorded by a Bruker Alpha II spectrometer (4000−500 cm^{-1}). A Bruker D8 advanced diffractometer using Cu Kα radiation was used for phase identification. Samples were mounted on a flat steel and scanned from 5 to 70°. A JEOL HRTEM-2100 electron microscope was used to get HRTEM images and selected area electron diffraction (SAED) patterns. SEM images were obtained by a ZEISS EVO LS 15 electron microscope. A Perkin Elmer Lambda 25 spectrometer (200−700 nm) was used to record the absorption spectra. Emission spectra were recorded using a Perkin Elmer LS 45 fluorescence spectrometer.

■ ASSOCIATED CONTENT

Supporting Information

The Supporting Information is available free of charge at https://pubs.acs.org/doi/10.1021/acsomega.2c07490.

Unit cell packing diagram $[Zn_2(dalldtc)_4]$, unit cell packing diagram of $[Ag_3(dalldtc)_3]$, FTIR spectra of $[Zn_2(dalldtc)_4]$ and $[Ag_3(diallyDTC)_3]$, electronic spectra of $[Zn_2(dalldtc)_4]$ and $[Ag_3(diallyDTC)_3]$, SEM images of zinc sulfide and silver sulfide nanoparticles capped with different capping agents, absorption spectra of zinc sulfide and silver sulfide nanoparticles, Tauc plots of zinc sulfide and silver sulfide nanoparticles capped with different capping agents, emission spectra of zinc sulfide and silver sulfide nanoparticles capped with different capping agents, and some selected bond lengths and bond angles for $[Zn(dalldtc)_4]$ (1) and $[Ag_3(dalldtc)_3]$ (2) (PDF)

Accession Codes

CCDC 2124746 and 2125073 contain the supplementary crystallographic data for this paper. The data can be obtained free of charge at www.ccdc.cam.ac.uk/structures or from the Cambridge Crystallographic Data Centre, 12 Union Road, Cambridge, CB2 1EZ, UK; fax: (+44)-1223-336-033.

■ AUTHOR INFORMATION

Corresponding Author

Peter A. Ajibade − *School of Chemistry and Physics, University of KwaZulu-Natal, Pietermaritzburg 3209, South Africa;* orcid.org/0000-0002-8581-2387; Email: ajibadep@ukzn.ac.za

Authors

Thandi B. Mbuyazi − *School of Chemistry and Physics, University of KwaZulu-Natal, Pietermaritzburg 3209, South Africa*

Athandwe M. Paca − *School of Chemistry and Physics, University of KwaZulu-Natal, Pietermaritzburg 3209, South Africa*

Complete contact information is available at: https://pubs.acs.org/10.1021/acsomega.2c07490

Notes

The authors declare no competing financial interest.

■ ACKNOWLEDGMENTS

The authors would like to thank the National Research Foundation (NRF) South Africa for the award of a competitive funding for rated researcher (Grant number 129275).

■ REFERENCES

(1) Andrew, F. P.; Ajibade, P. A. Metal complexes of alkyl-aryl dithiocarbamates: Structural studies, anticancer potentials and applications as precursors for semiconductor nanocrystals. *J. Mol. Struct.* **2018**, *1155*, 843−855.

(2) Buac, D.; Schmitt, S.; Ventro, G.; Rani Kona, F.; Ping Dou, Q. Dithiocarbamate-based coordination compounds as potent proteasome inhibitors in human cancer cells. *Mini Rev. Med. Chem.* **2012**, *12*, 1193−1201.

(3) Tan, Y. S.; Yeo, C. I.; Tiekink, E. R. T.; Heard, P. J. Dithiocarbamate complexes of platinum group metals: Structural aspects and applications. *Inorganics* **2021**, *9*, 60.

(4) Sulaiman, A. A. A.; Sobeai, H. M. A.; Aldawood, E.; Abogosh, A.; Alhazzani, K.; Alotaibi, M. R.; Ahmad, S.; Alhoshani, A.; Isab, A. A. In

vitro and in vivo studies of potential anticancer agents of platinum(II) complexes of dicyclopentadiene and dithiocarbamates. *Metallomics* **2022**.*14*, DOI: 10.1093/mtomcs/mfac054,

(5) Calabro, D. C.; Harrison, B. A.; Palmer, G. T.; Moguel, M. K.; Rebbert, R. L.; Burmeister, J. L. Thiocyanation, selenocyanation, and halogenation reactions of dithiocarbamate complexes of gold(I) and silver(I). Generation of gold(II) and silver(II) complexes. *Inorg. Chem.* **1981**, *20*, 4311−4316.

(6) Ajibade, P. A.; Fatokun, A. A.; Andrew, F. P. Synthesis, characterization, and anticancer studies of Mn(II), Cu(II), Zn(II) and Pt(II) dithiocarbamate complexes-crystal structures of the Cu(II) and Pt(II) complexes. *Inorg. Chim. Acta* **2020**, *504*, 119431.

(7) Ali, H.; Van Lier, J. E. Metal complexes as photo-and radiosensitizers. *Chem. Rev.* **1999**, *99*, 2379−2450.

(8) Zhu, J.-F.; Zhu, Y.-J.; Ma, M.-G.; Yang, L.-X.; Gao, L. Simultaneous and rapid microwave synthesis of polyacrylamide-metal sulfide (Ag_2S, Cu_2S, HgS) nanocomposites. *J. Phys. Chem. C* **2007**, *111*, 3920−3926.

(9) Selvaganapathi, P.; Thirumaran, S.; Ciattini, S. Synthesis, spectra, crystal structures and anticancer studies of 26 membered macrocyclic dibutyltin(IV) dithiocarbamate complexes: Single source precursors for tin sulfide nanoparticles. *Appl. Organomet. Chem.* **2019**, *33*, 1−14.

(10) Soliman, M. H.; Mohamed, G. G. Cr (III), Mn (II), Fe (III), Co (II), Ni (II), Cu (II) and Zn(II) new complexes of 5-aminosalicylic acid: spectroscopic, thermal characterization and biological activity studies. *Spectrochim. Acta, Part A* **2013**, *107*, 8−15.

(11) Assadullah, I.; Bhat, A. A.; Malik, J. H.; Malik, K. A.; Tomar, R. Optical, anticancer, photoluminescent, and electrochemical properties of crystalline ZnS quantum dots. *Energy Stor. Mater.* **2022**, *4*, No. e318.

(12) Rodríguez Padrón, D.; Puente Santiago, A. R.; Balu, A. M.; Muñoz Batista, M. J.; Luque, R. Environmental catalysis: present and future. *Chem. Cat. Chem.* **2019**, *11*, 18−38.

(13) Mohan, H.; Vadivel, S.; Rajendran, S. Removal of harmful algae in natural water by semiconductor photocatalysis-A critical review. *Chemosphere* **2022**, *302*, 134827.

(14) Paumo, H. K.; Dalhatou, S.; Katata-Seru, L. M.; Kamdem, B. P.; Tijani, J. O.; Vishwanathan, V.; Kane, A.; Bahadur, I. TiO2 assisted photocatalysts for degradation of emerging organic pollutants in water and wastewater. *J. Mol. Liq.* **2021**, *331*, 115458.

(15) Ahmed, S. N.; Haider, W. Heterogeneous photocatalysis and its potential applications in water and wastewater treatment: A review. *Nanotechnology* **2018**, *29*, 342001.

(16) Ayodhya, D.; Veerabhadram, G. A review on recent advances in photodegradation of dyes using doped and heterojunction based semiconductor metal sulfide nanostructures for environmental protection. *Mater. Today Energy* **2018**, *9*, 83−113.

(17) Munyai, S.; Hintsho-Mbita, N. Green derived metal sulphides as photocatalysts for waste water treatment. A review. *Curr. Opin. Green Sustain. Chem.* **2021**, *4*, 100163.

(18) Wang, J.; Sun, J.; Huang, J.; Fakhri, A.; Gupta, V. K. Synthesis and its characterization of silver sulfide/nickel titanate/chitosan nanocomposites for photocatalysis and water splitting under visible light, and antibacterial studies. *Mater. Chem. Phys.* **2021**, *272*, 124990.

(19) Onwudiwe, D. C.; Ajibade, P. A.; Omondi, B. Synthesis, spectral and thermal studies of 2,2'-bipyridyl adducts of bis(N-alkyl-N-phenyldithiocarbamato zinc(II). *J. Mol. Struct.* **2011**, *987*, 58−66.

(20) Al-Shehri, B. M.; Shkir, M.; Bawazeer, T. M.; AlFaify, S.; Hamdy, M. S. A rapid microwave synthesis of Ag2S nanoparticles and their photocatalytic performance under UV and visible light illumination for water treatment applications. *Physica E Low Dimens. Syst. Nanostruct.* **2020**, *121*, 114060.

(21) Stroyuk, A. L.; Raevskaya, A. E.; Korzhak, A. V.; Kuchmii, S. Y. Zinc sulfide nanoparticles: spectral properties and photocatalytic activity in metals reduction reactions. *J Nanopart. Res.* **2007**, *9*, 1027−1039.

(22) Memon, A. A.; Afzaal, M.; Malik, M. A.; Nguyen, C. Q.; O'Brien, P.; Raftery, J. The N-alkyldithiocarbamato complexes $[M(S_2CNHR)_2]$-(M= Cd (II) Zn (II); R= C_2H_5, C_4H_9, C_6H_{13}, $C_{12}H_{25}$); their synthesis, thermal decomposition and use to prepare of nanoparticles and nanorods of CdS. *Dalton Trans.* **2006**, *37*, 4499−4505.

(23) Motevalli, M.; O'Brien, P.; Walsh, J. R.; Watson, I. M. Synthesis, characterization and x-ray crystal structures of asymmetric bis (dialkyldithiocarbamates) of zinc: Potential precursors for ZnS deposition. *Polyhedron* **1996**, *15*, 2801−2808.

(24) Onwudiwe, D. C.; Ajibade, P. A. Synthesis and characterization of metal complexes of N-alkyl-N-phenyl dithiocarbamates. *Polyhedron* **2010**, *29*, 1431−1436.

(25) Shahid, M.; Rüffer, T.; Lang, H.; Awan, S. A.; Ahmad, S. Synthesis and crystal structure of a dinuclear zinc(II)-dithiocarbamate complex, bis {[(μ^2-pyrrolidinedithiocarbamato-S,S')-(pyrrolidinedithiocarbamato-S,S') zinc(II)]. *J. Coord. Chem.* **2009**, *62*, 440−445.

(26) Zhang, Q.; Cao, R.; Hong, M.; Su, W.; Liu, H. Polynuclear silver compound formed from aggregation of Se^{2-} and Ag(I)-thiolate complex. Synthesis, structure and spectroscopic characterization of $Ag_{11}(\mu_5\text{-Se})(\mu_4\text{-Et}_2\text{NCS}_2)_3(\mu_3\text{-Et}_2\text{NCS}_2)_6$. *Inorg. Chim. Acta* **1998**, *277*, 171−176.

(27) Ehsan, M. A.; Khaledi, H.; Tahir, A. A.; Ming, H. N.; Wijayantha, K. U.; Mazhar, M. Synthesis and characterization of silver diethyldithiocarbamate cluster for the deposition of acanthite (Ag_2S) thin films for photoelectrochemical applications. *Thin Solid Films* **2013**, *536*, 124−129.

(28) Ahmed, A. A.; Aldaghri, O.; Salih, E. Y.; Ramizy, A.; Madkhali, N.; Alinad, T.; Ibnaouf, K. H.; Eisa, M. H. Optical characteristics of Al-doped ZnS thin film using pulsed laser deposition technique: the effect of aluminum concentration. *Chal. Lett.* **2022**, *19*, 381−388.

(29) Ajibade, P. A.; Oluwalana, A. E. Photocatalytic degradation of single and binary mixture of brilliant green and rhodamine B dyes by zinc sulfide quantum dots. *Molecules* **2021**, *26*, 7686−7716.

(30) Karimi, F.; Rajabi, H. R.; Kavoshi, L. Rapid sonochemical water-based synthesis of functionalized zinc sulfide quantum dots: study of capping agent effect on photocatalytic activity. *Ultrason. Sonochem.* **2019**, *57*, 139−146.

(31) Di, L.; Xian, T.; Sun, X.; Li, H.; Zhou, Y.; Ma, J.; Yang, H. Facile preparation of CNT/Ag_2S nanocomposites with improved visible and NIR light photocatalytic degradation activity and their catalytic mechanism. *Micromachines* **2019**, *10*, 503.

(32) Tan, L.; Liu, S.; Yang, Q.; Shen, Y. Facile assembly of oppositely charged silver sulfide nanoparticles into photoluminescent mesoporous nanospheres. *Langmuir* **2015**, *31*, 3958−3964.

(33) Wageh, S.; Al-Ghamdi, A. A.; Numan, A.; Iqbal, J. Silver sulfide nanoparticles incorporated into graphene oxide: an efficient electrocatalyst for the oxygen reduction reaction. *J. Mater. Sci.: Mater. Electron.* **2020**, *31*, 8127−8135.

(34) Kodigala, S. R. Structural Properties of I−III−VI2 Absorbers. In *Thin Films and Nanostructures*, Vol. *35*; Elsevier, 2010; pp 115-194.

(35) Xu, Y.; Duan, S.; Li, H.; Yang, M.; Wang, S.; Wang, X.; Wang, R. Au/$Ni_{12}P_5$ core/shell single-crystal nanoparticles as oxygen evolution reaction catalyst. *Nano Res.* **2017**, *10*, 3103−3112.

(36) Üzar, N.; Arikan, M. Ç. Synthesis and investigation of optical properties of ZnS nanostructures. *Bull. Mater. Sci.* **2011**, *34*, 287−292.

(37) Yadu, G.; Pateria, M. A.; Deshmukh, K. Study of Ho doped AgS thin films prepared by CBD method. *Mater. Sci. Pol.* **2020**, *38*, 206−213.

(38) Bhushan, M.; Jha, R.; Bhardwaj, R. Reduced band gap and diffusion controlled spherical n-type ZnS nanoparticles for absorption of UV-Vis region of solar spectrum. *J. Phys. Chem. Solids* **2019**, *135*, 109021.

(39) Noreen, H.; Iqbal, J.; Hassan, W.; Rahman, G.; Yaseen, M.; Rahman, A. U. Synthesis of graphene nanoplatelets/polythiophene nanocomposites With Enhanced Photocatalytic Degradation of Bromophenol Blue and Antibacterial Properties. *Mater. Res. Bull.* **2021**, *142*, 111435.

(40) Ajibade, P. A.; Oluwalana, A. E.; Sikakane, B. M.; Singh, M. Structural, photocatalytic and anticancer studies of hexadecylamine capped ZnS nanoparticles. *Chem. Phys. Lett.* **2020**, *755*, 137813.

https://doi.org/10.1021/acsomega.2c07490
ACS Omega 2023, 8, 24750−24760

(41) Ajibade, P. A.; Solomane, N. Synthesis and crystal structure of bis(thiomorpholinyldithiocarbamato) Zn(II): structural, optical, and photocatalytic studies of ZnS nanoparticles from the complex. *J. Coord. Chem.* **2020**, *73*, 1292−1305.
(42) Di, L.; Xian, T.; Sun, X.; Li, H.; Zhou, Y.; Ma, J.; Yang, H. Facile Preparation of CNT/Ag_2S Nanocomposites with Improved Visible and NIR Light Photocatalytic Degradation Activity and Their Catalytic Mechanism. *Micromachines* **2019**, *10*, 503.
(43) Kisała, J.; Ferraria, A. M.; Mitina, N.; Cieniek, B.; Krzemiński, P.; Pogocki, D.; Nebesnyi, R.; Zaichenko, O.; Bobitski, Y. Photocatalytic activity of layered MoS_2 in the reductive degradation of bromophenol blue. *RSC Adv.* **2022**, *12*, 22465−22475.
(44) Ahmed, A.; Usman, M.; Yu, B.; Shen, Y.; Cong, H. Sustainable fabrication of hematite (α-Fe_2O_3) nanoparticles using biomolecules of Punica granatum seed extract for unconventional solar-light-driven photocatalytic remediation of organic dyes. *J. Mol. Liq.* **2021**, *339*, 116729.
(45) Khan, H.; Khalil, A. K.; Khan, A.; Saeed, K.; Ali, N. Photocatalytic degradation of bromophenol blue in aqueous medium using chitosan conjugated magnetic nanoparticles. *Korean J. Chem. Engineer.* **2016**, *33*, 2802−2807.
(46) Dolomanov, O. V.; Bourhis, L. J.; Gildea, R. J.; Howard, J. A. K.; Puschmann, H. OLEX2: a complete structure solution, refinement and analysis program. *J. Appl. Crystallogr.* **2009**, *42*, 339−341.
(47) Sheldrick, G. M. Crystal structure refinement with SHELXL. *Acta Crystallogr* **2015**, *71*, 3−8.
(48) Sheldrick, G. M. SHELXT−Integrated space-group and crystal-structure determination. *Acta Crystallogr* **2015**, *71*, 3−8.
(49) Paca, A. M.; Ajibade, P. A. Bis-(*N*-ethylphenyldithiocarbamato)-palladium(II) as molecular precursor for palladium sulfide nanoparticles. *J. Mol. Struct.* **2021**, *1243*, 130777.
(50) Ajibade, P. A.; Botha, N. L. Structural and optical studies of silver sulfide nanoparticles from silver(I) dithiocarbamate complex: molecular structure of ethylphenyl dithiocarbamato silver(I). *J. Sulfur Chem.* **2020**, *41*, 657−671.
(51) Ajibade, P. A.; Sikakane, B. M.; Botha, N. L.; Oluwalana, A. E.; Omondi, B. Synthesis and crystal structures of bis(dibenzyl dithiocarbamato)Cu(II) and Ag(I) complexes: Precursors for $Cu_{1.8}S$ and Ag_2S nano-photocatalysts. *J. Mol. Struct.* **2020**, *1221*, 128791.

https://doi.org/10.1021/acsomega.2c07490
ACS Omega 2023, 8, 24750−24760